Ecological Modelling
March 2024, Volume 489 Pages 110626 (13p.)
https://doi.org/10.1016/j.ecolmodel.2024.110626
https://archimer.ifremer.fr/doc/00872/98406/

Assessing regional connectivity patterns of bivalvia in fragmented archipelagos: Insights from biophysical modeling in French Polynesia

Raapoto Hirohiti [1], Monaco Cristián J. [1], Van Wynsberge Simon [1, 2], Le Gendre Romain [2], Le Luyer Jeremy [1, 3, *]

[1] Ifremer, IRD, Institut Louis-Malardé, Univ Polynésie française, EIO, F-98719 Taravao, Tahiti, Polynésie française, France
[2] Ifremer, UMR 9220 ENTROPIE (IRD, Univ. Réunion, IFREMER, Univ. Nouvelle-Calédonie, CNRS), BP 32078, 98897 Nouméa Cedex, New Caledonia
[3] Ifremer, Univ Brest, CNRS, IRD, LEMAR, Plouzané, 29280, Brest, France

* Corresponding author : Jeremy Le Luyer, email address : jeremy.le.luyer@ifremer.fr

Abstract :

Larval dispersal and connectivity are key processes that drive marine metapopulation dynamics, and therefore should be well characterized when designing effective management strategies. While temperature and food availability can structure marine species connectivity patterns, their contribution has not been thoroughly investigated in highly fragmented archipelagos. We used biophysical modeling of larval dispersal to explore the connectivity patterns of species with complex life-cycles across French Polynesia (FP), a territory formed by more than a hundred small, geographically isolated islands covering an area as large as Europe. We first simulated ten years of larval dispersal to investigate the spatial and temporal (seasonal and interannual) variability in larval dispersal pathways for different hypothetical species exhibiting a range of Larval Precompetency Period (LPP) values. Then, using the black-lip pearl oyster (Pinctada margaritifera) as a model species, we accounted for variability in the LPP induced by temperature and food availability, as derived from a Dynamic Energy Budget (DEB) model. The model showed that food availability and mesoscale turbulence (eddies) in the Marquesas jointly constrained larval dispersal, reducing its potential connectivity with other archipelagos in FP. The DEB simulations also revealed seasonal and interannual variability in connectivity driven by environmental conditions. However, accounting for food and temperature effects on larval development, barely changed the connectivity pattern at regional scale due to the remoteness of this archipelago. Our study thus provides appropriate management units definition at regional scale for the species across FP.

Highlights

► Food availability and mesoscale turbulence in the Marquesas jointly constrained larval dispersal, reducing its potential connectivity with other archipelagos in French Polynesia. ► Settlement success is influenced by climatic ENSO cycles that drive ocean currents in the Pacific region. ► Biophysical modelling refines management unit's definition in extremely fragmented archipelagos.

Keywords : Larval dispersal, Connectivity, Dynamic energy budget, Graph -theory, Network

1 Introduction

Demographic connectivity as defined by the exchange of individuals among geographically distinct populations, is vital for the persistence of metapopulations (Williams and Hastings, 2013), for the recovery of depleted populations following perturbations (Lipcius et al., 2008), and for maintaining genetic diversity (Trakhtenbrot et al., 2005). Characterizing larval dispersal and connectivity patterns of marine species is therefore crucial for quantifying population dynamics and to support effective resource-management policies (Cowen et al., 2007; Kritzer and Sale, 2004; Lipcius et al., 2008). However, assessing connectivity in marine systems remains a challenging task because most marine species have complex life histories involving planktonic larval stages.

Various methods exist to infer marine population connectivity, including genetic approaches (Lowe and Allendorf, 2010), geochemical markers (e.g. microchemical signatures in shells), *in situ* larval sampling techniques, or larval dispersal through hydrodynamic or biophysical modelling (see review in Jahnke and Jonsson, 2022). While empirical methods are often inadequate for species occurring across large geographic ranges, especially hyper-fragmented archipelagos, biophysical models emerge as suitable because they can account for both large spatial and temporal scales. Lagrangian models in particular, which allow the displacement of individual particles, are increasingly used for a wide range of applications (van Sebille et al., 2018) including describing the trajectory of marine debris, guiding search and rescue operations, estimating the age of water masses (Deleersnijder et al., 2001), and mapping the dispersion (Wood et al., 2016) and connectivity of marine larvae (Quinn et al., 2017; Wolanski et al., 2021).

Following Lagrangian models, the population connectivity of marine organisms with planktonic larval stage can be formalized as the probability of transport between two sites. This depends mainly on (i) the speed and direction of transport, as determined by oceanographic currents for planktonic larvae, and (ii) the Pelagic Larval Duration (PLD; i.e., time spent drifting before settlement). The PLD varies substantially across species and environmental conditions (from few hours to >100 days; (O'Connor et al., 2007). The lower limit of a species' PLD is determined by the Larval Pre-competency Period (LPP; also known as settlement-competency period), defined as the minimum time required for the larva to be able to settle. Once LPP is reached, larvae can fix as long as they reach adequate habitat conditions (O'Connor et al., 2007; Shima and Swearer, 2009; Wilson and Harrison, 1998). LPP is genetically controlled (species-specific) but it is also a plastic trait that varies considerably in response to environmental conditions, which can have important consequences for larval connectivity. For example, if warm temperatures accelerate larval development, the LPP and larval dispersal are reduced and connectivity patterns can be altered (O'Connor et al., 2007; Raventos et al., 2021). While the importance of temperature variability is generally acknowledged in larval connectivity models, few studies consider the role of food availability in larval development and growth (Sangare et al., 2020) And even though LPP or PLD are often included in biophysical models of dispersion, values are typically fixed based on empirical observations in controlled environments, thus rarely considering the dynamic environment encountered by larvae in the wild. An elegant and increasingly popular approach to account explicitly for the influence of temperature and food availability on larval dispersal is to combine biophysical and bioenergetic models, which is now possible thanks to recent advances in the fields of physical oceanography and physiological ecology (Falcini et al., 2020; Garavelli et al., 2016). Dynamic Energy Budget (DEB) models (Kooijman, 2009) provide powerful means to estimate LPP based on the local temperature and food conditions

105 experienced by individual larvae, thus potentially improving the predictions from biophysical dispersion models (Flores-Valiente et al., 2023; Sangare et al., 2019, 2020).

The French Polynesian (FP) territory provides an interesting playground to investigate larval dispersal and population connectivity patterns because of its sheer size (comparable to
110 that of Europe) and the presence of numerous islands organized in five highly-fragmented archipelagos that provide a diversity of environmental conditions. Even though the tropical ocean is typically characterized by a low productivity, higher temperature, and a weaker seasonal signal than temperate latitudes (Claustre et al., 2008; Dufour et al., 1999), large inter-archipelago variation exist in FP, notably between the Marquesas and the Gambier.
115 Furthermore, ocean circulation and environmental conditions are influenced on a seasonal scale but also on an interannual scale. Climate patterns such as ENSO (El Niño - Southern Oscillation) are known to impact the physico-chemistry of the Pacific Ocean (Delcroix, 1998; Gouriou and Delcroix, 2002; McPhaden and Zhang, 2004). Thus, such forcing might affect larval dispersal and connectivity in the area. Few studies, however, have aimed to quantify
120 larval dispersal and connectivity in the region (but see Martinez et al., 2007 for macroalgae drifts). While intra-lagoon larval dispersal has been examined for some FP atolls by either coupling hydrodynamic and bioenergetic models or by combining hydrodynamic and genetics information (Reisser et al., 2019), this has not been done across the whole of FP.

125 A quantitative understanding of the hydrodynamic and biological forces driving population connectivity across FP is of particular interest when considering its various bivalve species. These mollusks play significant roles in the local marine ecosystems, particularly in the benthic habitats. They are instrumental in the cycling of nutrients and contribute to the overall productivity of the marine environment (Vaughn and Hoellein, 2018). Among the many

130 species of bivalves present in FP, the black-lip pearl oyster (*Pinctada margaritifera*) is a species of high cultural and economic value that supports the local pearl industry (Andréfouët et al., 2012). *Pinctada margaritifera* has been the focus of numerous research projects, and significant contributions on population genetics provide insights into the potential degree of genetic structuring at basin scale (Lal et al., 2017) and also within and across FP atolls (Arnaud-
135 Haond et al., 2004, 2008; Lemer and Planes, 2014; Reisser et al., 2019). This work, however, is limited because even though it can describe the existing genetic structure of populations to infer connectivity, it is unable to unravel the ecological processes that produce them.

In this study, we first use biophysical modeling and graph-theory to explore overall larval
140 dispersal patterns in FP for different LPP values that are relevant for a wide range of species. We run these simulations over ten years to specifically investigate the spatial extent, the seasonal influence, and the interannual variability of larvae trajectories. Then, using *P. margaritifera* as model species, we computed the same dispersal simulations but using LPP as estimated from an along-track temperature- and food-dependent DEB model. This coupled
145 biophysical-bioenergetics model allows, for the first time, exploring the role of temperature and food availability on the connectivity patterns of sessile broadcast-spawner species across FP islands.

2 Methods

2.1 Study area

150 FP, located in the tropical South Pacific (155°W-130°W, 5°S-30°S; Fig. 1), is a vast territory spread over an area as large as Europe (~4.5 million km^2). Organized in 5 archipelagos with a total of 118 volcanic islands and atolls (Duncan and McDougall, 1976), only a small fraction of FP sits above sea level (4,200 km^2, <0.1 % of total area). Islands and atolls display extraordinary geomorphological variation, ranging in size between <1 and ~2,000 km^2

(Andréfouët et al., 2001; Galzin et al., 1994; Rougerie et al., 2004). While most of the Polynesian atolls and islands have a lagoon, high islands forming the northernmost archipelago (Marquesas) do not because of their drowned reefs (Rougerie et al., 1997). For islands and atolls that have lagoons, the degree of connectedness between the lagoon and ocean vary considerably from open to close, depending on the presence, number, and characteristics of reef passes and of shallow channels that cross the atoll rim (called *hoa*).

2.2 Biophysical modeling and ocean data

To build the biophysical model for FP, we used current velocity and temperature data from the Mercator Ocean global ocean reanalysis (GLORYS12V1) product, which provides daily data (interpolated to a higher temporal resolution for the Lagrangian experiment – see section **Erreur ! Source du renvoi introuvable.** *Lagrangian particle tracking*) on a spatial horizontal resolution of 1/12° (~9 km) and across 50 vertical levels. This product is available through the Copernicus Marine Environment Monitoring Service (CMEMS, https://marine.copernicus.eu/) described by (Lellouche et al., 2018). For this study, we averaged current velocities and temperatures across the first 50 meters to match the vertical distribution of *P. margaritifera* larvae (Thomas et al., 2012a,b) and to ensure manageable computing time. This also provide a more general picture of the flow field and thermal conditions that larval particles are likely to experience. Chlorophyll-*a* concentration data (Chl-a), a proxy for phytoplankton biomass (i.e., food availability for the larvae) were extracted from the product Copernicus-GlobColour based on multi-satellite observations, which provides daily estimates with a 4-km resolution (Maritorena et al., 2010). All data used in this study were extracted for the 2010-2019 period.

2.3 Lagrangian particles tracking

To model the Lagrangian drift of larvae we used the software Ocean Parcels (Delandmeter and Van Sebille, 2019; Lange and van Sebille, 2017). Ocean Parcels has been used in a variety of oceanographic applications (Escalle et al., 2019; Onink et al., 2019; Scutt Phillips et al., 2018; van Sebille et al., 2019), and was parameterized in this study as follows:

2.3.1 Particles emission

For the whole study period (2010-2019), 100 particles were released daily from each of the 102 biggest islands of FP. Islands that were in close proximity (< 2 km; i.e., Ravahere-Marokau) or those with a shared lagoon (i.e., Mangareva, Raiatea-Tahaa) were considered as one unique island. Particle initial positions were generated randomly from a 2-km buffer area extending between the crest of the outer reef and the reef slope. The locations of reef geomorphological units were extracted from the Millennium Coral Reef Mapping Product (MCRMP; Andréfouët et al., 2006). A total of 10,200 particles per day were released, representing a total of 37,250,400 particles for the 10 years of simulation (i.e., 365,200 per island).

2.3.2 Particle drift

In Ocean Parcels we set the time step of iteration to 1 hour and the position of larvae was recorded every 3 hours, which is lower than the ratio of cell size (9 km) to maximum current velocity in the area (~20 cm s^{-1}). This prevents particles to cross more than one boundary or hydrodynamic cell in a single time step and thus, prevents missing positions that might reach the small islands. Advection was simulated using a fourth-order Runge-Kutta integration scheme. Current velocity at the particle location was obtained through spatial and temporal linear interpolation of the flow field data. Because the resolution of the hydrodynamic forcing does not properly resolve dispersion related to turbulent eddies, a stochastic 'random walk' impulse was applied to each modelled larva (Quinn et al., 2017; van Sebille et al., 2018).

Temperature and Chl-a at each particle location were obtained through spatial and temporal linear interpolation and recorded every 3 hours.

Once LPP was reached (see section 2.4 *Larval dispersal scenarios tested*), we allowed particles to settle as soon as they crossed a patch of suitable habitat (i.e., hard substrate surrounding an island or atoll). Because most FP islands are too small to be properly captured by the resolution of GLORYS data, masks of hard substrates were designed on the basis of MCRMP and used to determine when particles reached suitable habitat. Larvae were considered as settled when they entered a 2-km buffer zone around these masks (same as defined for the initial positions). We tracked particles for a maximum of 35 days, as this encompasses the PLD for many tropical marine species, including *P. margaritifera* (Sangare et al., 2019; Thomas et al., 2014). Beyond this period of 35 days, particles that did not encounter a suitable habitat were considered lost.

2.4 Larval dispersal scenarios tested

Nine scenarios were considered to investigate the relative importance of LPP and environmental conditions in the global connectivity patterns. A baseline scenario (scenario 0) forced larvae to drift until the end of the simulation (35 days), to assess the maximal extent of the dispersal kernel that can be expected considering current velocity and direction in FP.

A set of 7 scenarios included connectivity matrices for a wide range of marine species exhibiting a spectrum of LPPs (and maximum PLD; PLD_{max}), from 3 to 23 days (Table 1). The LPP was fixed to two thirds of the PLD_{max} in our scenarios to consider the fact that the longer the pre-competent period, the greater the capacity for delaying metamorphosis (Pechenik, 1990; Wellington and Victor, 1989).

The eighth scenario specifically considered the case study of *P. margaritifera*. We determined the LPP of each simulated larva based on predictions from a Dynamic Energy Budget model for the species (Sangare et al., 2020; see section *2.5. Spatial DEB modeling to determine LPP*). In all scenarios, no mortality curve nor predation were simulated.

Scenario	Settlement parametrization	LPP (days)	PLD_{max} (days)
0	No-settlement scenario	-	35
1	Settlement as soon as crossing suitable habitat when LPP reached	3	5
2		7	10
3		10	15
4		13	20
5		17	25
6		20	30
7		23	35
8		From DEB	35

Table 1: larval pre-competency period (LPP) and maximum pelagic larval duration (PLDmax) for the eight scenarios considered in this study

2.5 Spatial DEB modeling to determine LPP

To determine the effective pre-competency period of each individual larva of *P. margaritifera* released in our simulations (scenario 8), we estimated growth and development using dynamic energy budget theory (Kooijman, 2009). Based on a robust theoretical framework that is consistent with and can explain long-standing empirical models in biology (e.g., von Bertalanffy growth) (Sousa et al., 2010), DEB theory allows quantifying the energy use and allocation of organisms experiencing variable environmental conditions (temperature and food availability). Throughout the life of an organism, DEB models can explicitly predict key life-history traits including growth, reproduction, and notably maturity level (Monaco et

al., 2014). Here we used the DEB model described for *P. margaritifera* by Sangare et al. (2020, 2019); parameter values available at https://www.bio.vu.nl/thb/deb/deblab/add_my_pet/entries_web/Pinctada_margaritifera/Pincta da_ margaritifera_res.html), which has been calibrated and validated using data on larva and adult life stages (Fournier, 2011; Thomas et al., 2011). The model considers that larvae grow exponentially until reaching a maturity threshold that marks the onset of metamorphosis, thus defining the end of the LPP. We began each simulation with new-born larvae that then drifted in the water column following the modelled Lagrangian trajectories. At each daily time step, we estimated the larva size and maturity depending on the sea surface temperature and Chl-a data. Since our DEB model does not allow a proper definition of PLD_{max}, the same previous statement was used for linking LPP and PLD_{max} (PLD_{max} defined as three halves the LPP). Once particles reached this value, they were considered lost.

2.6 Data analysis

Dispersal and connectivity metrics. First, the probability of transport from an island or group of islands *i* to an island or group of islands *j* ($P_{i \to j}$) was calculated as the proportion of larvae emitted from the island *i* that settled at *j*. Then, four larval dispersal metrics (Lett et al., 2015) were calculated based on $P_{i \to j}$, at the scale of the islands. The settlement success for island *i* (SS_i) was calculated as the proportion of particles emitted from *i* that could settle (either in the same island/group of islands or elsewhere; eq. 1), while the recruitment success (RS_i) for an island *i*, is the ratio of the number of particles settled on *i* and the total number of particles emitted from the whole dataset on the time period considered (eq. 2). Local retention at island *i* (LR_i) is defined by $P_{i \to i}$, and self-recruitment (SR_i) is the ratio of locally produced settlement to settlement of all origins at a site (eq. 3).

$$SS_i = \sum_{j=1}^{n} P_{i \to j} \quad \text{(eq. 1)}$$

$$RS_{i,t} = \frac{\sum_{j=1}^{n}(P_{j\to i} \times N_j)}{\sum_{j=1}^{n} N_j} \quad \text{(eq. 2)}$$

$$SR_i = \frac{P_{i\to i} \times N_i}{\sum_{j=1}^{n}(P_{j\to i} \times N_j)} \quad \text{(eq. 3)}$$

With N_i *and* N_j the number of larvae emitted from island *i* and *j* respectively, considered equal in this study.

2.6.1 Seasonal and interannual trends

A seasonality analysis was performed on the total RS from all islands to determine the monthly recruitments. They were obtained by computing the average and standard deviation on monthly data over the 10 years of simulation. To visualize interannual dispersal trends, monthly recruitments (RS) were filtered with the STL (Seasonal-Trend decomposition procedure based on Loess) additive scheme (Cleveland et al., 1990). This filtering procedure decomposes a time series into trends, seasonal and remaining components, which is particularly appropriate for extracting the interannual and trend signals from non-stationary and noisy climate datasets (Terray, 2011). The STL procedure decomposes the analyzed X(t) monthly time series into three terms:

$$X(t) = T(t) + A(t) + R(t)$$

The T(t) term quantifies the trend and low-frequency variations in the time series. The A(t) term describes the annual cycle and its modulation through time. Finally, R(t) is the residual term containing the interannual signal and the noise present in the data. A comparison of RS trends and the Southern Oscillation Index (SOI) was also performed to assess the possible

295 influence of ENSO on larval dispersion. The SOI data were retrieved from the NOAA dataset (https://www.cpc.ncep.noaa.gov/data/indices/soi).

2.6.2 Network analysis

We used a network analysis based on graph theory (Koutrouli et al., 2020) on the probability
300 of transport from an island *i* to an island *j* ($P_{i \to j}$) to i) explore connectivity patterns across islands over the 10-year study period (2010-2019), ii) identify putative island clusters based on *degree* metrics and iii) compare the clustering across the 8 scenarios with settlement (Table 1). Briefly, each node in our network corresponds to islands or atolls in FP (n = 102; supp. Table 1) while directed edges (*from*, *to*) represent mean dispersal rates across nodes. The overall
305 network connectivity was estimated, and common graph metrics were assessed for each node to identify atolls or islands of priority for resource management purposes. First, we used the *network density* (ratio of observed edges to the number of possible edges in the network) as a proxy of overall network fragmentation. We used the node's *degree* (the number of connections ingoing and outgoing from a node) as a measure of the importance of the node to act as source
310 or sink. Finally, we explored sub-structuring (i.e., clusters) based on the hierarchical Louvain's method (Blondel et al., 2008). All network analyses were conducted with the *scikit-network* python library (Bonald et al., 2020). Dispersal metrics (SS, RS, LR and SR) previously computed at the scale of the islands were also computed at the scale of the clusters i.e group of islands) and the archipelagos. For testing differences across clusters or islands, we used yearly
315 values and non-parametrical Kruskal-Wallis rank sum tests. Pairwise comparison tests were then computed using Wilcoxon rank sum exact tests and Bonferroni correction.

3 Results

3.1 Spatial and temporal patterns of temperature, food, and currents

The surface ocean circulation mainly followed the south pacific gyre over the study period. In the northern part of the area, the South Equatorial Current (SEC) flowing westward/southwestward was the main current affecting FP and was stronger around the Marquesas archipelago with yearly average velocities around 20 cm s^{-1}, compared to 10 cm s^{-1} in the rest of the area (Figure 1b).

The yearly mean ocean temperature averaged across the upper 50 meters ranged between 22°C in the Austral archipelago and 28°C in the western Tuamotu and Society islands (Figure 1c). In the north-east area, the imprint of the equatorial upwelling induces slightly colder waters (< 27.5 °C). While in the north-west, the south-eastward imprint of the warm pool induces slightly warmer water (> 28 °C).

Oceanic water masses in FP are nutrient-depleted with low Chl-a concentrations (Figure 1d). The mean surface Chl-a shows a south-west/north-east gradient due to the contribution of nutrient-rich waters from the equatorial upwelling. The highest values are observed around the Marquesas archipelago.

The variability and spatial patterns of ocean temperature and surface Chl-a remain relatively constant, primarily due to the location of French Polynesia in the tropical region. However, it is noteworthy that a slightly stronger variability is observed in the southern region.

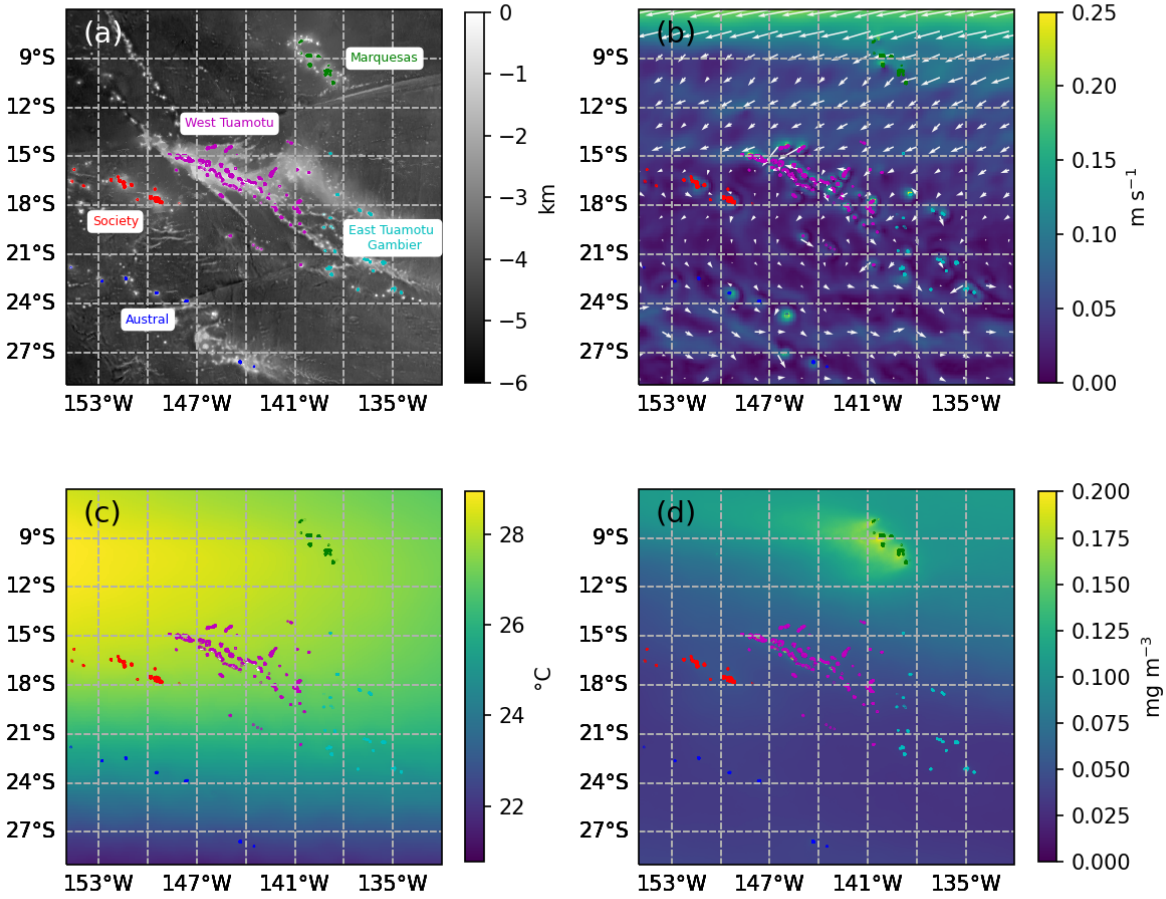

Figure 1: a) Bottom topography of FP with the Marquesas (green), Western Tuamotu (pink), Society (red), Eastern Tuamotu – Gambier (cyan), and Austral (dark blue) archipelagos. (b) Mean current speed (b) and (c) temperature averaged over 2010 to 2019 across the first 50 m depth from Mercator Ocean global reanalysis (GLORYS12V1). (d) Mean surface chlorophyll-a averaged on the same time period from Global Ocean Colour (GlobColour) data.

3.2 Potential particle dispersal over 35 days (Scenario 0)

For the 10 years of simulation, the maximum dispersal distance of particles that drifted for 35 days ranged from 0 to 1463 km (scenario 0; Figure 2). This scenario predicted high

isolation of the Austral and Marquesas archipelagos, but high connections between the other archipelagos. In this scenario, relatively few particles emitted from the Society archipelago could reach the Austral and West Tuamotu archipelagos (Figure 2b), and none could reach the Marquesas and East Tuamotu-Gambier archipelagos. Particles from the West Tuamotu islands dispersed randomly, albeit a slight south-westward shift of the maximum distribution (Figure 2c), presumably associated to the main current (Figure 1b). West Tuamotu particles reach most of the islands from the Society and East Tuamotu-Gambier archipelagos. Particles from the East Tuamotu-Gambier archipelago spread northwestward but could reach the Tuamotu West only (Figure 2d). Larvae released from the Marquesas archipelago, which is the most affected by the SEC (Figure 1b), tend to spread south-westward. However, they could hardly reach the West Tuamotu in 35 days (Figure 2e). Similarly, particles emitted from the Austral could not reach the other archipelagos in 35 days (Figure 2f).

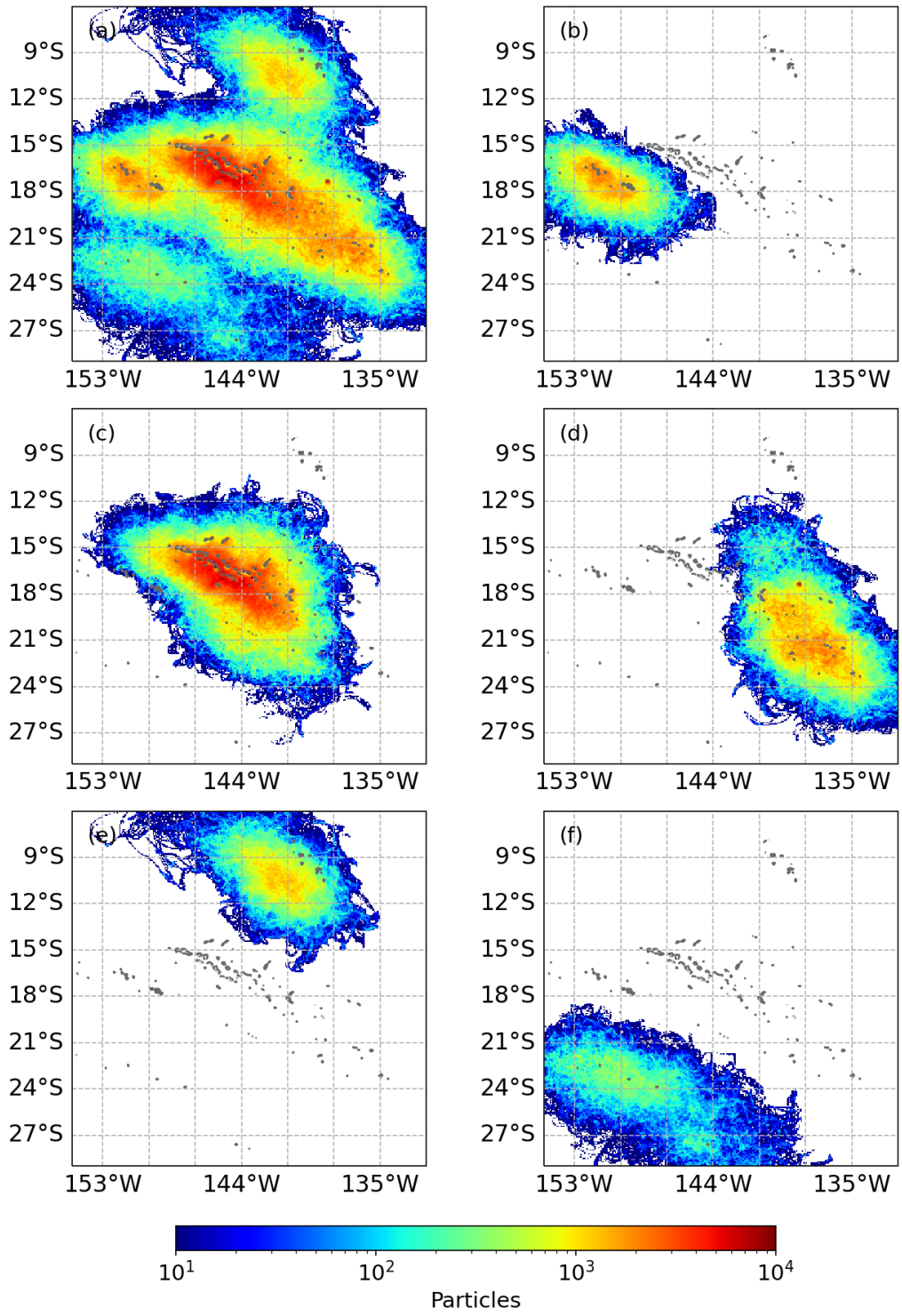

360

Figure 2: Simulated dispersal distributions after a duration of 35 days without settlement (scenario 0), expressed as larval densities and calculated as the number of particles in each cell on a 1/100° grid for (a) all FP, (b) larvae emitted from the Society only, (c) from the West Tuamotu only, (d) from the East Tuamotu-Gambier, (e) from the Marquesas, and (f) from the

365 *Austral archipelagos. Note that in this scenario the positions of larvae exclude mortality or settlement. Animation for FP can be viewed in the Supplementary Materials section.*

3.3 Potential connectivity across a range of LPP scenarios (scenarios 1 to 7)

After ten years of simulation, out of the 37,250,400 particles generated all over FP, only 370 2.10 and 8.04 % larvae reached a suitable substrate for LPP scenarios of 3 and 23 days, respectively (Table 2). Mean total recruitment success (RS) and mean distance traveled increased linearly with LPP (Table 2).

Scenario	LPP (days)	SS (%)	RS (%)	SR (%)	LR (%)	Distance of settlement to source (km)	Correlation between SOI and SS	p-value	Number of clusters
1	3	2.10 ± 0.16 ^{e}	0.02 ± 0.00 ^{e}	63.30 ± 3.17 ^{f}	1.22 ± 0.14 ^{b}	27.83 ± 2.57 ^{f}	-0.55	5.15 10^{-11}	42
2	7	3.04 ± 0.15 ^{f}	0.03 ± 0.00 ^{f}	48.82 ± 3.07 ^{g}	1.39 ± 0.15 ^{bc}	59.47 ± 5.16 ^{g}	-0.44	3.98 10^{-7}	25
3	10	4.86 ± 0.27 ^{a}	0.05 ± 0.00 ^{a}	40.22 ± 2.57 ^{a}	1.72 ± 0.20 ^{a}	89.89 ± 7.03 ^{a}	-0.60	7.07 10^{-13}	19
4	13	6.18 ± 0.35 ^{b}	0.06 ± 0.00 ^{b}	34.51 ± 2.56 ^{b}	1.74 ± 0.21 ^{a}	122.04 ± 9.95 ^{b}	-0.61	1.31 10^{-13}	14
5	17	6.28 ± 0.45 ^{bc}	0.06 ± 0.00 ^{bc}	29.86 ± 1.87 ^{c}	1.47 ± 0.20 ^{abc}	157.67 ± 13.02 ^{c}	-0.49	9.54 10^{-9}	12
6	20	7.25 ± 0.57 ^{cd}	0.07 ± 0.00 ^{cd}	26.53 ± 1.70 ^{d}	1.42 ± 0.20 ^{abc}	188.78 ± 15.13 ^{d}	-0.41	2.71 10^{-6}	11
7	23	8.04 ± 0.64 ^{d}	0.08 ± 0.01^{d}	23.70 ± 1.02 ^{e}	1.36 ± 0.18 ^{bc}	220.04 ± 17.99 ^{e}	-0.38	1.49 10^{-5}	10
8	DEB	8.65 ± 0.99 ^{d}	0.08 ± 0.01 ^{d}	25.35 ± 1.67 ^{de}	1.63 ± 0.28 ^{ac}	193.34 ± 1.68 ^{d}	-0.21	0.02	12

Table 2: Total mean settlement success (SS), recruitment success (RS), self-recruitment (SR), 375 *local retention (LR), distance of settlement to source, correlation between SS and Southern oscillation index (SOI) and number of clusters over the 10 years of simulation for the various scenarios. Letters indicate significance at Bonferroni adjusted $P < 0.05$. The number of clusters is computed on 10 years of simulation.*

Monthly settlements revealed no apparent seasonal trend emerging from the different scenarios 1 to 7 (Figure 3a). The settlement trend obtained through the STL analysis is shown in Figure 3b (see Supp Mat for the observed, seasonal, and residual signals). All scenarios with a fixed LPP show the lowest SS in 2011, when the SOI is highly positive (La Niña), and the highest in 2014, when the SOI is becoming negative (El Niño). Indeed, both signals from settlements and SOI present a weak negative correlation for all seven scenarios (Table 2). Low SS trend was also found in 2011 for scenario 8 (DEB), but the lowest SS was obtained in 2017 for this scenario, when the SOI was moderately positive (La Niña).

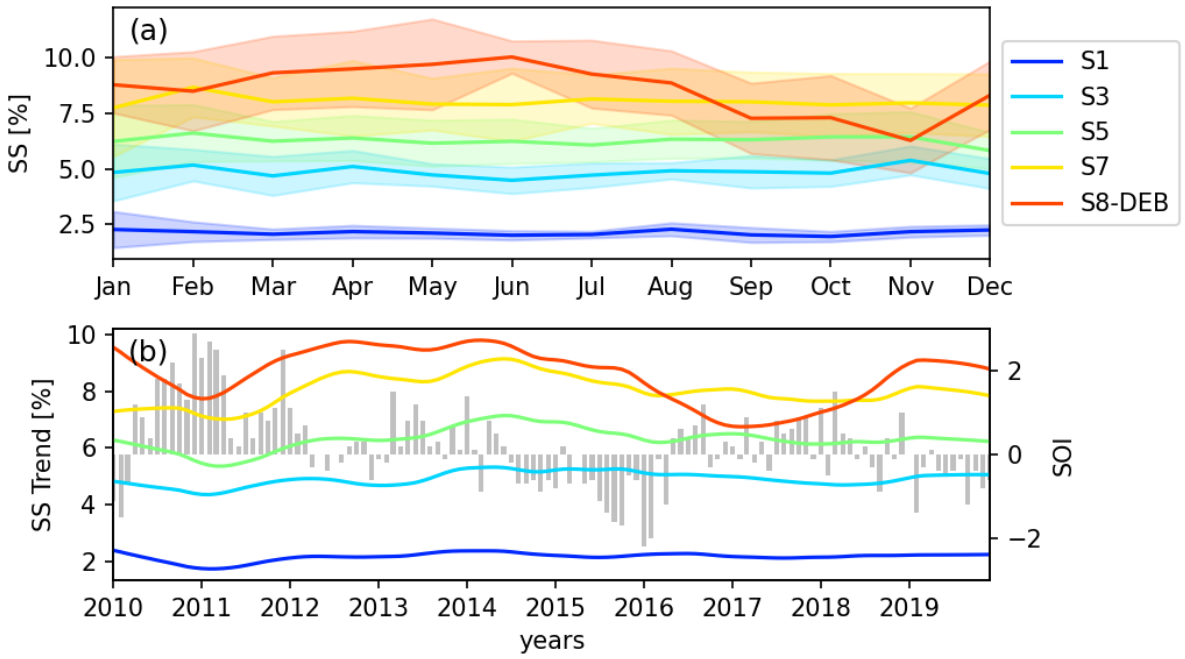

Figure 3: (a) Time series of the monthly average SS, with shades representing their standard deviations and (b) the interannual SS trend extracted from the STL over the full dataset (all archipelagos included). For ease of representation, only scenarios 1, 3, 5, 7 and 8 are represented in dark blue, cyan, green, yellow and orange, respectively. The SOI is represented in gray bar plot for the same period.

Potential connectivity matrices for LPP of 3, 10, 17 and 23 days, as well as the DEB model-derived LPP, are shown in Figure 4. For the shortest LPP (3 days), apart SR, only few connections were possible with neighboring islands (Table 2 and Figure 4a). Indeed, the mean traveled distance for these particles was around 28 km (Table 2). Therefore, only very close group of islands might share larvae such as those in the Western Tuamotu. With longer LPP, potential connectivity matrices were more complex with connections appearing between more distant islands and exports being possible between different archipelagos (Figure 4b, c, and d).

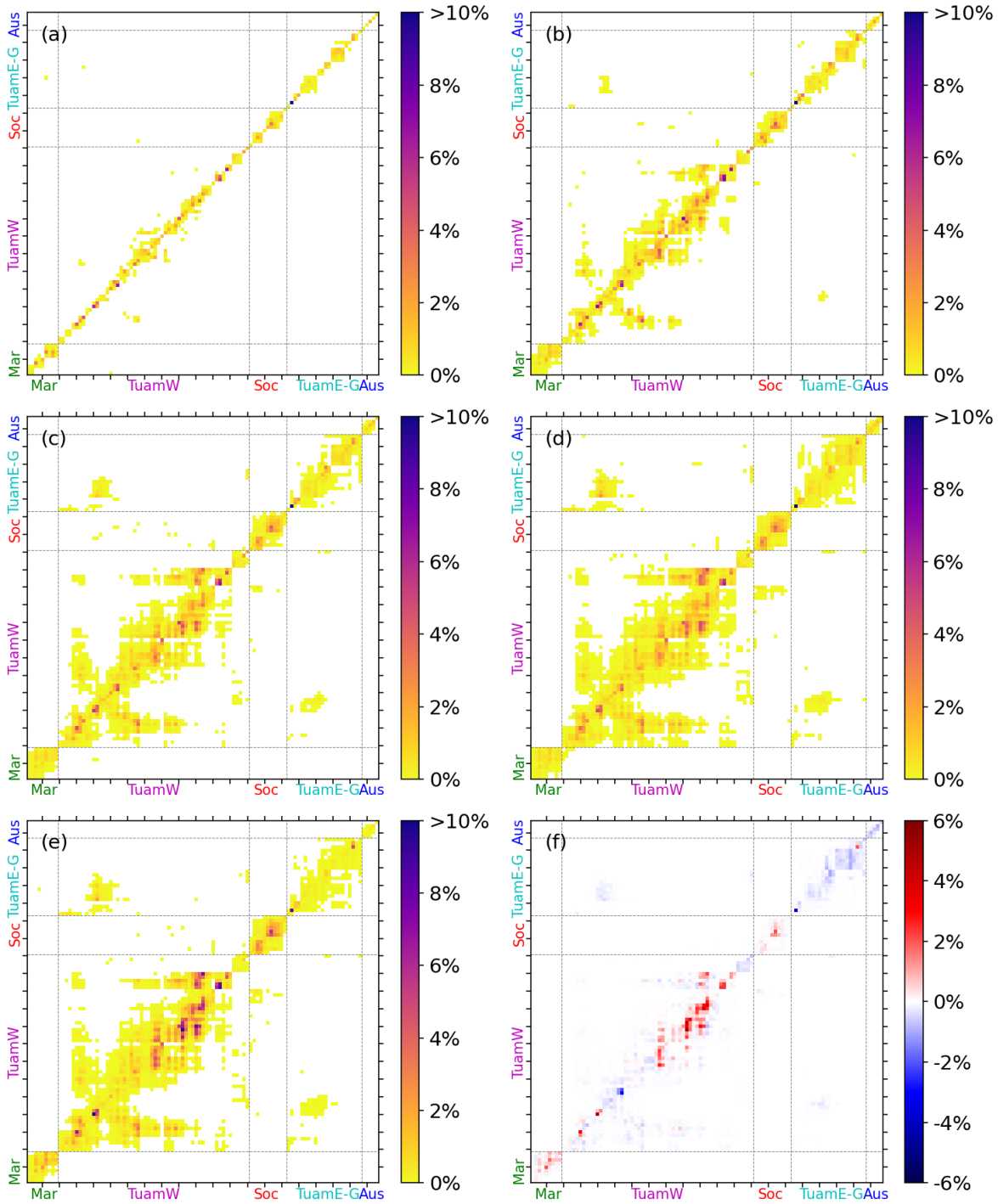

405 *Figure 4: Potential connectivity matrices for (a) scenario 1 (LPP of 3 days), (b) scenario 3 (LPP of 10 days), (c) scenario 5 (LPP of 17 days), (d) scenario 7 (LPP of 23 days) and (e) scenario 8 (LPP based on the DEB model). The difference between scenario 8 and 7 is shown in (f). Source islands are on the left axis and destination islands on the bottom one. Indexes from the Marquesas (Mar), Western Tuamotu (TuamW), Society (Soc), Eastern Tuamotu -*

Gambier (TuamE-G), and Austral (Aus) archipelagos are colored in green, pink, red, cyan, and dark blue, respectively. The islands in the matrices are sorted according to the main ocean currents (see Supp Table 1)

For the 10 years of simulation, network fragmentation decreased with increasing LPP as shown by the reduction of the number of clusters and linear increase in network density (Figure 5a). Years 2011 (La Niña) and 2013/2014 had the minimum and maximum network density, respectively (Figure 5a).

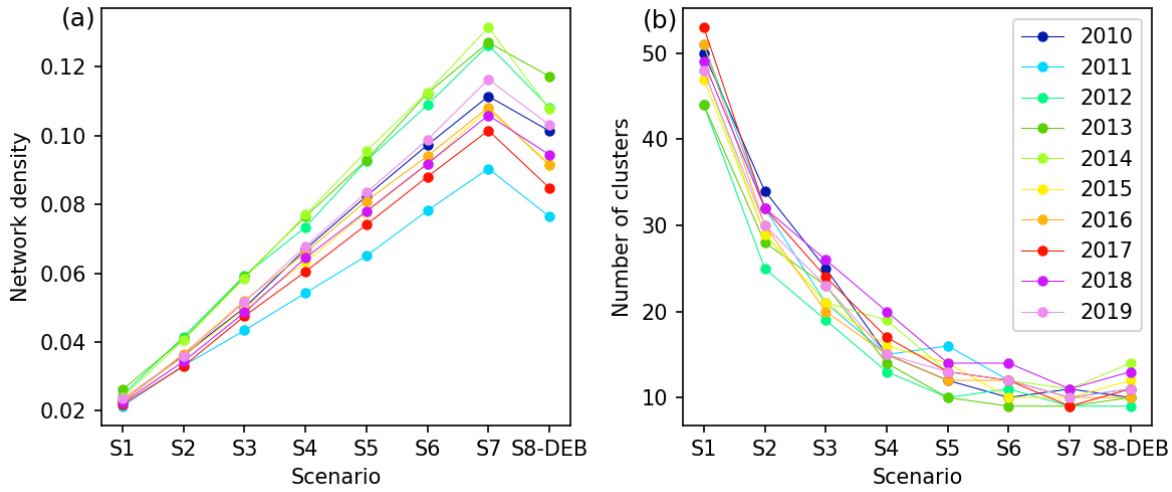

Figure 5: (a) Network density and (b) number of clusters per year and according to the different scenarios. Points were joined with lines for better visualization.

Islands and atolls grouped into clusters are shown in Figure 6 and the total number of clusters identified for each scenario over the 10 years in Table 2. For 3-day LPP (i.e., 5-day maximum PLD; scenario 1), islands were grouped in 42 clusters with the largest one formed by 11 (out of 102) islands (Figure 6a). As LPP increased, the clusters were joined together to form larger components, increasing the overall connectivity in FP. At the longest PLD_{max} (35

days), islands were grouped into 10 clusters, with the largest one formed by 28 islands (27.4% - black in Figure 6d). The region being so fragmented, none of the configurations presented here allowed the system to be fully connected.

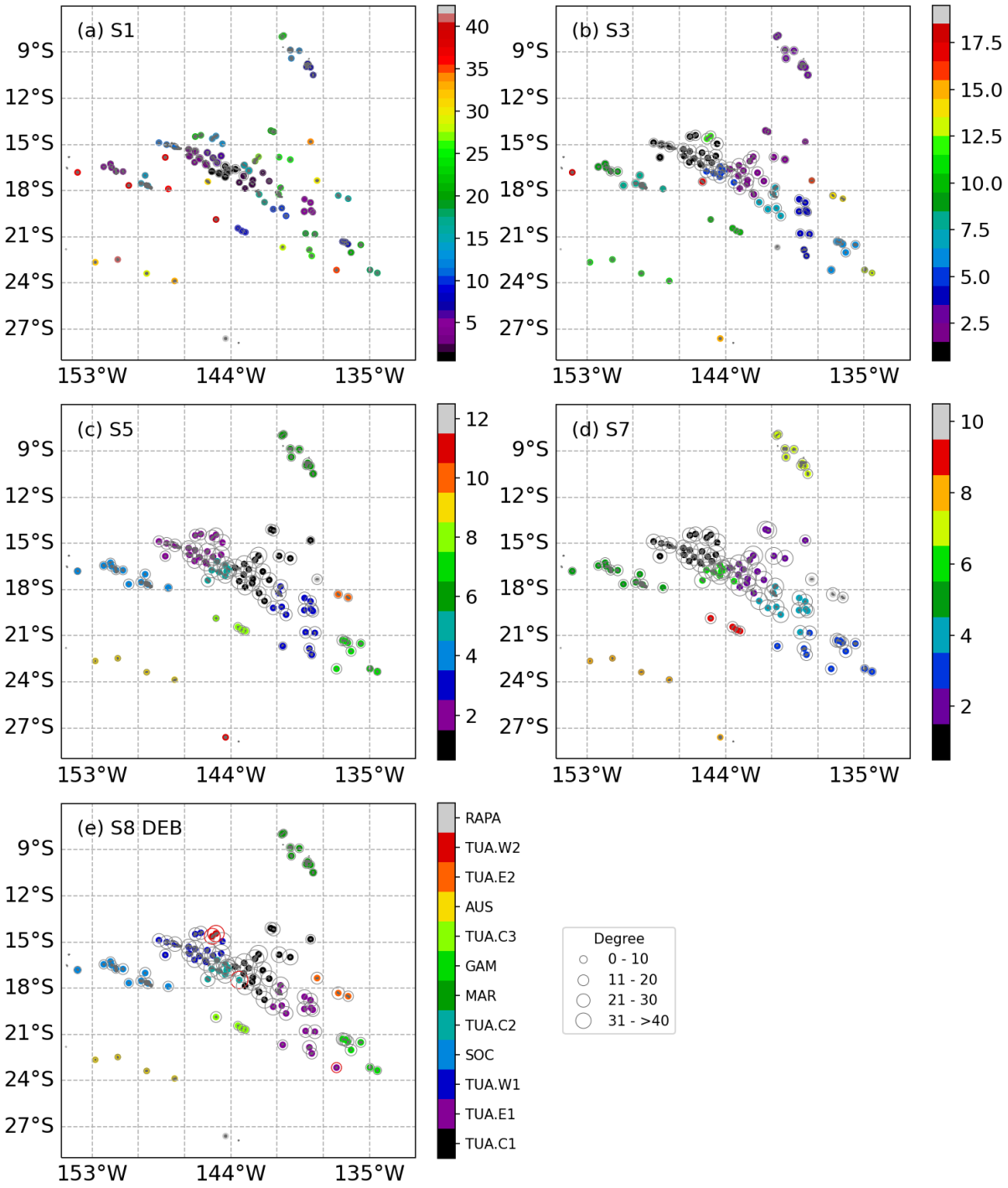

Figure 6: Cluster distributions over the 10-year simulation dataset for (a) scenario 1, (b) scenario 3, (c) scenario 5 and (d) scenario 7 and (e) scenario 8 (DEB). Colors refer to clusters sorted from the largest to the smallest one from bottom to top. Grey circles refer to the number of degree. In (e), circles in red represent the islands that changed clusters between scenario 5 and scenario 8.

3.4 *Pinctada margaritifera* connectivity (Scenario 8)

At FP scale, the LPP obtained from the DEB model increased southward, with a minimum of 11.55 days for Marquesas islands and reaching >27-30 days for Austral islands, Gambier islands, and the southeastern part of Tuamotu archipelago (Table 3). Both seasonal and interannual variations of SS for *P. margaritifera* were stronger than for the fixed LPP scenarios (Figure 3). The potential connectivity matrix is comparable to the one from scenario 7 with a fixed LPP of 23 days (Figure 4d and 4e). However, by considering environmental influences on LPP, potential connectivity increases within the Marquesas and western Tuamotu archipelagos (2-5%) while it generally decreases in the others (Figure 4f). Network clustering based on connectivity matrices computed using the DEB model over the 10 years simulated provided 12 different clusters (Figure 6e). The Society (SOC), Gambier (GAM) and Marquesas (MAR) archipelagos were well delimited. Austral (AUS) archipelago was identified as a separate cluster, but its remotest island Rapa formed a cluster on its own while the Tuamotu archipelago was divided in 7 clusters. These patterns are close to those observed in scenario 5 with a fixed LPP of 17 days (Figure 6c); however, some differences were observed among the islands. Some of them formed new clusters on their own in scenario 8 (DEB) such as Takaroa and Takapoto in the western Tuamotu. While the others changed from one to another in the eastern Tuamotu (Morane) and in the central Tuamotu (Haraiki). Average SS varied across clusters (K-W Chi-squared = 57.7, $P < 0.001$), ranging from 0.18% ± 0.20 to 30.61% ± 4.27

for RAPA and TUA.W2, respectively (Table 3). Similarly, RS varied largely across clusters (K-W Chi-squared = 114.88, $P < 0.001$), with again an almost null RS for RAPA, while maximum RS was observed for TUA.W1 (Table 3). SR varied across clusters (K-W Chi-squared = 109.78, $P < 0.001$), reaching 100% for AUS, RAPA and MAR in scenario 8 (DEB). LR was higher in the West Tuamotu (TUA.W1 and TUA.W2) reaching 16.74 ± 1.67 and 14.10 ± 6.53, respectively (Table 3). TUA.C2 showed the highest degree value, indicative of the centrality of the cluster for the network (Table 3).

Clusters	SS (%)	SR (%)	LR (%)	RS (%)	Degree	Distance to settlement (km)	LPP (days)
AUS	0.43 ± 0.27^{a}	100 ± 0.00^{a}	0.43 ± 0.27^{a}	0.01 ± 0.01^{a}	3.50	96.15 ± 50.03^{abc}	29.5 ± 6.60^{abcd}
GAM	1.77 ± 0.44^{b}	96.85 ± 4.35^{bcde}	1.64 ± 0.45^{b}	0.13 ± 0.04^{b}	15.50	92.24 ± 30.04^{abc}	28.0 ± 1.25^{a}
MAR	3.73 ± 1.40^{c}	100.00 ± 0.00^{ab}	3.73 ± 1.40^{c}	0.33 ± 0.12^{c}	8.67	50.45 ± 7.74^{a}	11.5 ± 1.42^{e}
RAPA	0.18 ± 0.20^{a}	100.00 ± 0.00^{ab}	0.12 ± 0.20^{a}	0.00 ± 0.00^{d}	1	5.77 ± 3.23	30.0 ± 12.89^{abcde}
SOC	7.00 ± 1.04^{de}	98.13 ± 2.11^{c}	6.99 ± 1.03^{de}	0.77 ± 0.11^{e}	12.45	73.62 ± 11.96^{b}	22.5 ± 0.96^{bc}
TUA.C1	9.31 ± 1.39^{d}	83.07 ± 7.86^{f}	6.59 ± 1.14^{de}	1.41 ± 0.27^{f}	33.55	120.63 ± 8.89^{c}	23.5 ± 2.81^{bcd}
TUA.C2	14.70 ± 2.84^{f}	61.75 ± 6.52^{g}	9.43 ± 1.74^{df}	1.49 ± 0.19^{f}	36.40	76.81 ± 13.46^{b}	23.5 ± 2.13^{bc}
TUA.C3	0.67 ± 0.47^{a}	88.03 ± 8.73^{cdef}	0.66 ± 0.46^{a}	0.03 ± 0.02^{a}	10.75	59.39 ± 32.92^{ab}	30.0 ± 2.62^{ad}
TUA.E1	3.49 ± 1.54^{bc}	79.11 ± 14.62^{dfg}	3.09 ± 1.34^{bc}	0.60 ± 0.20^{ce}	24.68	100.68 ± 18.13^{bc}	27.0 ± 2.51^{abd}
TUA.E2	4.30 ± 2.64^{ce}	97.97 ± 2.69^{abce}	4.39 ± 2.55^{bce}	0.13 ± 0.07^{b}	17.33	55.82 ± 28.91^{abc}	24.5 ± 2.46^{abcd}
TUA.W1	19.16 ± 2.48^{f}	76.87 ± 3.57^{d}	16.74 ± 1.67^{g}	3.42 ± 0.37^{g}	27.81	88.12 ± 7.72^{b}	20.5 ± 2.50^{c}
TUA.W2	30.61 ± 4.27^{g}	86.05 ± 7.22^{def}	14.10 ± 6.53^{fg}	0.32 ± 0.13^{c}	33.00	90.77 ± 27.41^{bc}	20.0 ± 2.72^{c}

Table 3: Summary statistics for theoretical dispersal based on DEB model for P. margaritifera (scenario 8) and 10 years computation (2010-2019). Letters represent significant differences across clusters at Bonferroni adjusted $P < 0.05$.

4 Discussion

4.1 Connectivity in FP and consequences for management

Ocean connectivity is one of the main drivers of metapopulation dynamics and evolution in marine organisms. Larval transport and dispersal potential are constrained both by i) hydro-physical properties of the environment, notably current transport, and by ii) genetic and phenotypically plastic properties of the organism which determine LPP and PLD. To assess the relative role of LPP on FP connectivity we used a Lagrangian particle dispersal model through 8 scenarios that considered various LPP and maximum PLD (from 5 to 35 days). Using a graph-theory framework (Treml et al., 2008), we showed that population fragmentation, estimated through overall network density and the number of identified clusters, decreased with increasing LPP and maximum PLD. The association between PLD and population connectivity has also been detected using population genetic approaches, notably based on isolation-by-distance (IBD) estimations derived from genetic data (Selkoe and Toonen, 2011; Treml et al., 2012). As PLD varies substantially in the marine realm, from 0 for lecitrophic to >100 days for some planktonic species (Mercier et al., 2013), our observation that the clustering of populations in FP depends on PLD highlights the importance of defining species-specific management units for fishery management and for live animal translocation for aquaculture purposes. Furthermore, we showed that FP archipelagos remain largely disconnected, even for the 35-days-maximum-PLD scenario, with 12 main clusters identified. Such isolation was also observed in other species like giant clams (*Tridacna maxima;* Laurent et al., 2002) whose LPPs are shorter than those of *P. margaritifera*. Nevertheless, considering the large scale of our study and possible bias at local scale (model resolution, local hydrodynamic circulations affecting all affecting local retention and settlement), we expect that connectivity patterns estimated in this study are more robust at archipelago scale, and detailed connectivity between islands inside archipelagoes should be interpreted with caution.

495

4.2 Environmental drivers of connectivity

Among the environmental conditions that could affect settlement rates and PLD, temperature has been one of the most studied in marine species (O'Connor et al., 2007; Raventos et al., 2021), and little attention has been given to the influence of food availability. Nevertheless, in FP, temperatures are relatively stable compared to temperate regions, suggesting that this might not be the main driver influencing PLD and connectivity (Sangare et al., 2020a). In turn, Chl-a concentration exhibits greater variability across the territory. Chl-a is significantly higher in the Marquesas than at any other archipelago due to a strong island mass effect, while temperature remains close to the optimal for *P. margaritifera* (Le Moullac et al., 2016; Raapoto et al., 2018, 2019). According to empirical observation and modeling for *P. margaritifera* (Sangare et al., 2020; Thomas et al., 2011), these environmental conditions decrease LPP and favor local retention of larvae, as has been previously documented (Raapoto et al., 2018). Our results support the observation of a segregation between the Marquesas and the rest of FP based on microsatellite data (Reisser et al., 2019).

Overall, our results suggest that the contribution of the environmental conditions to *P. margaritifera* clustering at the scale of FP is dampened, and connectivity is mainly driven by the geographical configuration of the archipelagos. The Marquesas archipelago (in the North) is isolated by both distance and short LPP due to Chl-a rich waters. The Austral archipelago (in the South) remains isolated from the rest of the network mainly because of geographical and hydrodynamical reasons. Even if temperature experienced by larvae in the area tend to extend their LPP, the main current flow and the remoteness of these islands prevent connectivity with other northern clusters. Finally, the islands of the Society and Tuamotu archipelagos form a denser group with homogeneous environmental conditions which lead to clustering patterns consistent with what is observed with the fixed 23-days-LPP scenarios. Our

analysis also revealed that, even though DEB model predictions do not enhance estimates of connectivity among highly-fragmented clusters, they do provide valuable information when considering dispersal metrics at narrower temporal and spatial scales. The variability in temperature and Chl-a modulates the settlement success at seasonal and interannual scales (Fig. 3), and can also identify clusters, such as Takaroa and Takapoto in the western Tuamotu (Fig. 6e), Takapoto being the main provider of spat for the pearl farming sector.

4.3 Consequence for management

Results from our model can inform science-based management practices. The pearl industry in FP depends on wild spat collection. A few atolls (5 to 6) provide most of the biological material to the 556 pearl producers across 26 atolls and islands (Ky et al. 2019). This system has favored the spread of parasites and diseases and led to the regulation of transfers [i.e., destination restricted to non-collecting atolls and limited to locally collected biological material in the Gambier archipelagos (Bondad-Reantaso et al., 2007; Chagot et al., 1993) and genetic homogenization (Lemer and Planes, 2012)]. We show that spat-collecting atolls, which are mainly located in the West Tuamotu, are the most central in the network, with elevated connectivity. Moreover, atoll connectivity help maintaining stable populations (Hughes, 1990), hence, informing on population resilience potential. Such information is vital for tropical ectotherm species leaving already close to their upper thermal limits (Hughes et al., 2003; Seebacher et al., 2015), and for enclosed lagoons which are sensitive to environmental degradation (Andréfouët et al., 2015; Rodier et al., 2019).

4.4 Relevance of the approach and results for other species and archipelagic countries

The dispersal modelling approach developed in this study was justified for *P. margaritifera*'s case study in FP, but might require adjustments if used for other species or archipelagos. First, the currents data (GLORYS) we used to force the Lagrangian model had a relatively coarse spatial and temporal resolution (~9 km; daily). Although FP islands are located in a low eddy-activity area (Chelton et al., 2007), the presence of obstacles in the flow field may induce turbulent flow downstream. Currents used here do not resolve sub-mesoscale dynamics around islands, which would allow to determine the proximity of particles to passes and their potential influx towards the lagoon. The low resolution of currents used in this study was of limited concern for characterizing the general patterns of connectivity at the scale of the territory, considering the wide distance between many islands in FP. Also, current velocities being averaged across the first 50 m depth, Stokes drift forcing is not considered in our experiment since its magnitude decrease rapidly with depth (Tamura et al., 2012). Implementing a similar approach in a less fragmented system, or at smaller scale, by contrast, may require adapting the resolution of the model to picture adequately the sub-mesoscale processes.

Second, in our model, particles were limited to a 2-dimensional displacement only. This was justified for *P. margaritifera* whose larvae distribution is light dependent so that larvae can maintain themselves in the upper layers of the water column (Thomas et al., 2012b), but this may be a limit to transpose results to species whose larvae occupy the water column differently.

Third, the dispersal kernels modelled in this study do not account for differences in population abundance between islands. Differences in populations abundance among islands do not change the probability of transport from an island i to an island j ($P_{i \rightarrow j}$), nor local

retention (LR), but may change estimates for other dispersal metrics calculated here (SS, RS, and SR), as well as the degree and number of clusters derived from graph theory. To date, *P. margaritifera* natural and farmed stocks have been assessed only for a few lagoons in FP (Andréfouët et al., 2016; Bionaz et al., 2022), which precludes us from integrating this variable into the dispersal models. While population size could be related with atoll size in other regions, this is not the case in FP (Andréfouët et al., 2016; Bionaz et al., 2022). Full estimates of *P. margaritifera* stocks would allow to weight larval emission by localization, and potentially improve the connectivity matrices (Falcini et al., 2020). Similar improvement would benefit from the inclusion of additional forces modulating effective connectivity (e.g., spawning, and larval and post-larval survival). Meanwhile, one can hypothesize that the pattern of connectivity estimated in this study (i.e., high isolation of populations in Marquesas and Austral archipelagos compared to other archipelagos) remain probably true, and is even more accentuated in reality.

Fourth, the percentage of larval export from the lagoon to oceanic waters might be linked to lagoon water renewal, which vary depending on the atoll's geomorphology (Andréfouët et al., 2022). In the semi-enclosed atoll lagoon of Ahe, larval export rate has been estimated to be ~40% (Andréfouët et al., 2021), while closed atolls are expected to export significantly less larvae (Andréfouët et al., 2001). Although the dispersal kernels we estimated do not consider the degree of openness of each island/atoll, our results provide a basis of dispersal patterns triggered by oceanic transport at the scale of the territory. This can contribute to finer-grain dispersal studies that will take local geomorphology and mesoscale circulation patterns into account.

Our model integrating spatial-DEB (scenario 8) identifies 12 clusters, which largely overlapped with existing archipelago-wise management units, and is congruent with previous genetic data for *P. margaritifera*. Specifically, our simulations clearly identify Gambier,

Marquesas and Austral islands as disconnected from the Tuamotu Archipelago, in accordance with previous genetic clustering studies for *P. margaritifera* (Lemer and Planes, 2014; Reisser et al., 2019). West Tuamotu atolls were at the center of the network showing the highest connectivity with surrounding atolls and islands. The archipelago itself was divided into 7 different clusters, but this was not detected with genetic data. The discrepancy is likely due to both the confounding effect of human transfers, and the different scales of observation used in our model and the population genetic approach (long time-scale observations *versus* single-step connectivity). Models accounting for dispersion with steppingstones and filial-coalescence connectivity, improved knowledge on spawning, and stock assessments would certainly help in resolving connectivity in the Tuamotu (Boulanger et al., 2020; Legrand et al., 2022).

4.5 Impact of climate change on larval dispersal

By examining the larval dispersal and connectivity patterns of different marine bivalve species including *P. margaritifera*, within FP islands on the 2010-2019 period, we found variable settlement success (SS) depending on ENSO cycles. Notably, lower SS were found during strong La Niña periods. This result raises the question of the potential impact of climate change on connectivity patterns in FP. Ocean warming is widely considered to be one of the major stressors to ocean ecosystems (Raventos et al., 2021). Rising temperature has a direct impact on larval development by decreasing PLD. At global scale, a PLD decrease of 10% to 25% is suspected (O'Connor et al., 2007; Raventos et al. 2021). Such decrease might isolate the Marquesas and Austral archipelago even more. Furthermore, this change in temperature may affect the timing of reproduction in many marine species, including *P. margaritifera.* The time lag induced by the temperature change might modify the connectivity and its variability for certain species (Lacroix et al., 2018). Furthermore, the frequency, intensity, and duration of marine heat waves is expected to increase in the future (Rahmstorf and Coumou, 2011). Similar approaches using DEB modeling but using ocean projection instead of hindcast data is

the next step to better capture the potential impact of these warming events on connectivity at regional scale. Given the homogeneous temperature pattern in FP, such perspective work should not only consider ocean temperature projection, but also the change in ocean circulation in response to climate change. Indeed, these changes in ocean conditions could also alter larval transport pathways, potentially affecting the dispersal patterns and genetic diversity of many species. Previous studies suggest that the change in ocean circulation might be the most prominent driver of the dispersal in a climate change context (Cetina-Heredia et al., 2015). Finally, climate change is likely to lead to a decrease in global phytoplankton biomass (Boyce et al., 2010). This decrease in phytoplankton could have significant repercussions on food availability for larvae development and thus extending their LPP. Therefore, it is important that future research continues to investigate the impact of climate change on larval dispersal and the implications for the genetic diversity and sustainability of marine species.

5 Conclusions

This paper assessed the influence of environmental conditions over the pelagic larval duration and population connectivity in marine organisms, with a focus on the black-lip pearl oyster *P. margaritifera* in FP. We used a Lagrangian particle dispersal model to recreate seven scenarios of maximum PLD ranging from 5 to 35 days and one scenario based on a DEB modeling approach. The graph-theory framework showed that even though these archipelagos are not fully connected, population fragmentation decreases with increasing PLD.

The wealth of biological data available for the local model species *P. margaritifera* allowed producing a biophysical dispersion model that explicitly considers the energetic condition of individual larvae, and predict settlement success. Even though the DEB model-derived predictions did not modify the regional clustering in FP, it did help explain the interannual and seasonal variability of settlement success. These results further highlight the

importance of accounting for variability in food and temperature for assessing the impacts of climate change over the regional connectivity.

The results indicate the importance of defining species-specific management units for fishery management and for live animal translocation for aquaculture purposes in FP and other archipelagic countries. Environmental drivers such as temperature and food availability were also discussed, with a focus on the influence of Chl-a concentration on local retention of larvae. Our approach lends itself for investigating the connectivity patterns of other species or regions, thus providing a valuable tool to improve our understanding of marine metapopulation dynamics and evolutionary processes.

REFERENCES

Andréfouët, S., Charpy, L., Lo-Yat, A., Lo, C., 2012. Recent research for pearl oyster aquaculture management in French Polynesia. Marine Pollution Bulletin 65, 407–414. https://doi.org/10.1016/j.marpolbul.2012.06.021

Andréfouët, S., Desclaux, T., Buttin, J., Jullien, S., Aucan, J., Le Gendre, R., Liao, V., 2022. Periodicity of wave-driven flows and lagoon water renewal for 74 Central Pacific Ocean atolls. Marine Pollution Bulletin 179, 113748. https://doi.org/10.1016/j.marpolbul.2022.113748

Andréfouët, S., Dutheil, C., Menkes, C.E., Bador, M., Lengaigne, M., 2015. Mass mortality events in atoll lagoons: environmental control and increased future vulnerability. Global Change Biology 21, 195–205. https://doi.org/10.1111/gcb.12699

Andréfouët, S., Le Gendre, R., Thomas, Y., Lo-Yat, A., Reisser, C.M.O., 2021. Understanding connectivity of pearl oyster populations within Tuamotu atoll semi-closed lagoons: Cumulative insight from genetics and biophysical modelling approaches. Marine Pollution Bulletin 167, 112324. https://doi.org/10.1016/J.MARPOLBUL.2021.112324

Andréfouët, S., Muller-Karger, F.E., Robinson, J.A., Torres-Pulliza, D., Spraggins, S.A., Murch, B., 2006. Global assessment of modern coral reef extent and diversity for regional science and management applications: a view from space. Proceedings of the 10th International Coral Reef Symposium, pp. 1732–1745.

Andréfouët, S., Pagès, J., Tartinville, B., 2001. Water renewal time for classification of atoll lagoons in the Tuamotu Archipelago (French Polynesia). Coral Reefs 20, 399–408. https://doi.org/10.1007/s00338-001-0190-9

Andréfouët, S., Thomas, Y., Dumas, F., Lo, C., 2016. Revisiting wild stocks of black lip oyster Pinctada margaritifera in the Tuamotu Archipelago: The case of Ahe and Takaroa atolls and implications for the cultured pearl industry. Estuarine, Coastal and Shelf Science 182, 243–253. https://doi.org/10.1016/j.ecss.2016.06.013

Arnaud-Haond, S., Vonau, V., Bonhomme, F., Boudry, P., Blanc, F., Prou, J., Seaman, T., Goyard, E., 2004. Spatio-temporal variation in the genetic composition of wild populations of pearl oyster (*Pinctada margaritifera cumingii*) in French Polynesia following 10 years of juvenile translocation. Molecular Ecology 13, 2001–2007. https://doi.org/10.1111/j.1365-294X.2004.02188.x

Arnaud-Haond, S., Vonau, V., Rouxel, C., Bonhomme, F., Prou, J., Goyard, E., Boudry, P., 2008. Genetic structure at different spatial scales in the pearl oyster (*Pinctada margaritifera cumingii*) in French Polynesian lagoons: beware of sampling strategy and genetic patchiness. Mar Biol 155, 147–157. https://doi.org/10.1007/s00227-008-1013-0

Bionaz, O., Le Gendre, R., Liao, V., Andréfouët, S., 2022. Natural stocks of *Pinctada margaritifera* pearl oysters in Tuamotu and Gambier lagoons: New assessments, temporal evolutions, and consequences for the French Polynesia pearl farming industry. Marine Pollution Bulletin 183, 114055. https://doi.org/10.1016/j.marpolbul.2022.114055

Blondel, V.D., Guillaume, J.-L., Lambiotte, R., Lefebvre, E., 2008. Fast unfolding of communities in large networks. J. Stat. Mech. 2008, P10008. https://doi.org/10.1088/1742-5468/2008/10/P10008

Bonald, T., Lara, N. de, Lutz, Q., Charpentier, B., 2020. Scikit-network: Graph Analysis in Python. Journal of Machine Learning Research 21, 1–6.

Bondad-Reantaso, M.G., McGladdery, S.E., Berthe, F.C.J., 2007. Pearl Oyster Health Management: A Manual 503.

Boulanger, E., Dalongeville, A., Andrello, M., Mouillot, D., Manel, S., 2020. Spatial graphs highlight how multi-generational dispersal shapes landscape genetic patterns. Ecography 43, 1167–1179. https://doi.org/10.1111/ecog.05024

Boyce, D.G., Lewis, M.R., Worm, B., 2010. Global phytoplankton decline over the past century. Nature 466, 591–596. https://doi.org/10.1038/nature09268

Cetina-Heredia, P., Roughan, M., van Sebille, E., Feng, M., Coleman, M.A., 2015. Strengthened currents override the effect of warming on lobster larval dispersal and survival. Global Change Biology 21, 4377–4386. https://doi.org/10.1111/gcb.13063

Chagot, D., Fougerouse, A., Weppe, M., Marques, A., Bouix, G., 1993. Presence of gregarine (Protozoa sporozoa) parasite of black-lipped pearl oysters *Pinctada margaritifera* (L.,1758) (Mollusca bivalvia) in French Polynesia. Comptes Rendus de L'academie des sciences. Serie III, Sciences de la vie 316, 239–244.

Chelton, D.B., Schlax, M.G., Samelson, R.M., de Szoeke, R.A., 2007. Global observations of large oceanic eddies. Geophysical Research Letters 34. https://doi.org/10.1029/2007GL030812

Claustre, H., Sciandra, A., Vaulot, D., 2008. Introduction to the special section Bio-optical and biogeochemical conditions in the South East Pacific in late 2004: the BIOSOPE program. Biogeosciences discussion 5, 605–640.

Cleveland, R.B., Cleveland, W.S., McRae, J.R., Terpenning, I., 1990. STL: A seasonal-trend decomposition procedure based on loess. Journal of official statistics 6, 3–73.

Cowen, R., Gawarkiewicz, G., Pineda, J., Thorrold, S., Werner, F., 2007. Population Connectivity in Marine Systems: An Overview. Oceanog. 20, 14–21. https://doi.org/10.5670/oceanog.2007.26

Delandmeter, P., Van Sebille, E., 2019. The Parcels v2.0 Lagrangian framework: new field interpolation schemes. Geosci. Model Dev. 12, 3571–3584. https://doi.org/10.5194/gmd-12-3571-2019

Delcroix, T., 1998. Observed surface oceanic and atmospheric variability in the tropical Pacific at seasonal and ENSO timescales: A tentative overview. Journal of Geophysical Research: Oceans 103, 18611–18633. https://doi.org/10.1029/98JC00814

Deleersnijder, E., Campin, J.-M., Delhez, E.J.M., 2001. The concept of age in marine modelling I. Theory and preliminary model results. Journal of Marine systems 28, 229–267.

Dufour, P., Charpy, L., Bonnet, S., Garcia, N., 1999. Phytoplankton nutrient control in the oligotrophic South Pacific subtropical gyre (Tuamotu Archipelago). Marine Ecology Progress Series 179, 285–290. https://doi.org/10.3354/meps179285

Duncan, R.A., McDougall, I., 1976. Linear volcanism in French Polynesia. Journal of Volcanology and Geothermal Research 1, 197–227. https://doi.org/10.1016/0377-0273(76)90008-1

Escalle, L., Scutt Phillips, J., Brownjohn, M., Brouwer, S., Sen Gupta, A., Van Sebille, E., Hampton, J., Pilling, G., 2019. Environmental versus operational drivers of drifting FAD

beaching in the Western and Central Pacific Ocean. Sci Rep 9, 14005. https://doi.org/10.1038/s41598-019-50364-0

Falcini, F., Corrado, R., Torri, M., Mangano, M.C., Zarrad, R., Di Cintio, A., Palatella, L., Jarboui, O., Missaoui, H., Cuttitta, A., Patti, B., Santoleri, R., Sarà, G., Lacorata, G., 2020. Seascape connectivity of European anchovy in the Central Mediterranean Sea revealed by weighted Lagrangian backtracking and bio-energetic modelling. Sci Rep 10, 18630. https://doi.org/10.1038/s41598-020-75680-8

Flores-Valiente, J., Lett, C., Colas, F., Pecquerie, L., Aguirre-Velarde, A., Rioual, F., Tam, J., Bertrand, A., Ayón, P., Sall, S., Barrier, N., Brochier, T., 2023. Influence of combined temperature and food availability on Peruvian anchovy (*Engraulis ringens*) early life stages in the northern Humboldt Current system: A modelling approach. Progress in Oceanography 215, 103034. https://doi.org/10.1016/j.pocean.2023.103034

Fournier, J., 2011. Alimentation et déterminisme environnemental de la reproduction des huîtres perlières *P. margaritifera* sur l'atoll d'Ahe (Archipel des Tuamotu, Polynésie Française) (PhD). Université de Polynésie Française, French Polynesia.

Galzin, R., Planes, S., Dufour, V., Salvat, B., 1994. Variation in diversity of coral reef fish between French Polynesian atolls. Coral Reefs 13, 175–180. https://doi.org/10.1007/BF00301196

Garavelli, L., Colas, F., Verley, P., Kaplan, D.M., Yannicelli, B., Lett, C., 2016. Influence of Biological Factors on Connectivity Patterns for *Concholepas concholepas* (loco) in Chile. PLoS ONE 11, e0146418. https://doi.org/10.1371/journal.pone.0146418

Gouriou, Y., Delcroix, T., 2002. Seasonal and ENSO variations of sea surface salinity and temperature in the South Pacific Convergence Zone during 1976–2000. Journal of geophysical research 107, SRF 12-1-SRF 12-14.

Hughes, T.P., 1990. Recruitment Limitation, Mortality, and Population Regulation in Open Systems: A Case Study. Ecology 71, 12–20.

Hughes, T.P., Baird, A.H., Bellwood, D.R., Card, M., Connolly, S.R., Folke, C., Grosberg, R., Hoegh-Guldberg, O., Jackson, J.B.C., Kleypas, J., Lough, J.M., Marshall, P., Nyström, M., Palumbi, S.R., Pandolfi, J.M., Rosen, B., Roughgarden, J., 2003. Climate Change, Human Impacts, and the Resilience of Coral Reefs. Science 301, 929–933. https://doi.org/10.1126/science.1085046

Jahnke, M., Jonsson, P.R., 2022. Biophysical models of dispersal contribute to seascape genetic analyses. Phil. Trans. R. Soc. B 377, 20210024. https://doi.org/10.1098/rstb.2021.0024

Kooijman, B., 2009. Dynamic Energy Budget Theory for Metabolic Organisation, 3rd ed. Cambridge University Press.

Koutrouli, M., Karatzas, E., Paez-Espino, D., Pavlopoulos, G.A., 2020. A Guide to Conquer the Biological Network Era Using Graph Theory. Frontiers in Bioengineering and Biotechnology 8.

Kritzer, J.P., Sale, P.F., 2004. Metapopulation ecology in the sea: from Levins' model to marine ecology and fisheries science. Fish and Fisheries 5, 131–140. https://doi.org/10.1111/j.1467-2979.2004.00131.x

Ky, C.-L., Broustal, F., Potin, D., Lo, C., 2019. The pearl oyster (*Pinctada margaritifera*) aquaculture in French Polynesia and the indirect impact of long-distance transfers and

collection-culture site combinations on pearl quality traits. Aquaculture Reports 13, 100182. https://doi.org/10.1016/j.aqrep.2019.100182

Lacroix, G., Barbut, L., Volckaert, F.A.M., 2018. Complex effect of projected sea temperature and wind change on flatfish dispersal. Global Change Biology 24, 85–100. https://doi.org/10.1111/gcb.13915

Lal, M.M., Southgate, P.C., Jerry, D.R., Bosserelle, C., Zenger, K.R., 2017. Swept away: ocean currents and seascape features influence genetic structure across the 18,000 Km Indo-Pacific distribution of a marine invertebrate, the black-lip pearl oyster *Pinctada margaritifera.* BMC Genomics 18, 66. https://doi.org/10.1186/s12864-016-3410-y

Lange, M., van Sebille, E., 2017. Parcels v0.9: prototyping a Lagrangian ocean analysis framework for the petascale age. Geoscientific Model Development 10, 4175–4186. https://doi.org/10.5194/gmd-10-4175-2017

Laurent, V., Planes, S., Salvat, B., 2002. High variability of genetic pattern in giant clam (*Tridacna maxima*) populations within French Polynesia. Biological Journal of the Linnean Society 77, 221–231. https://doi.org/10.1046/j.1095-8312.2002.00106.x

Le Moullac, G., Soyez, C., Latchere, O., Vidal-Dupiol, J., Fremery, J., Saulnier, D., Lo Yat, A., Belliard, C., Mazouni-Gaertner, N., Gueguen, Y., 2016. *Pinctada margaritifera* responses to temperature and pH: Acclimation capabilities and physiological limits. Estuarine, Coastal and Shelf Science, SI:Sustainable pearl-culture 182, Part B, 261–269. https://doi.org/10.1016/j.ecss.2016.04.011

Legrand, T., Chenuil, A., Ser-Giacomi, E., Arnaud-Haond, S., Bierne, N., Rossi, V., 2022. Spatial coalescent connectivity through multi-generation dispersal modelling predicts gene flow across marine phyla. Nat Commun 13, 5861. https://doi.org/10.1038/s41467-022-33499-z

Lellouche, J.-M., Bourdalle-badie, R., Garric, G., Drevillon, M., Regnier, C., Greiner, E., Le Galloudec, O., Melet, A., Bricaud, C., Hernandez, O., Drillet, Y., Le Traon, P.-Y., Hamon, M., 2018. The Copernicus Marine Environment Monitoring Service global ocean 1/12 physical reanalysis GLORYS12V1: description and quality assessment, in: EGU General Assembly Conference Abstracts. p. 19806.

Lemer, S., Planes, S., 2014. Effects of habitat fragmentation on the genetic structure and connectivity of the black-lipped pearl oyster *Pinctada margaritifera* populations in French Polynesia. Mar Biol 161, 2035–2049. https://doi.org/10.1007/s00227-014-2484-9

Lemer, S., Planes, S., 2012. Translocation of wild populations: conservation implications for the genetic diversity of the black-lipped pearl oyster *Pinctada margaritifera*. Molecular Ecology 21, 2949–2962. https://doi.org/10.1111/j.1365-294X.2012.05588.x

Lett, C., Nguyen-Huu, T., Cuif, M., Saenz-Agudelo, P., Kaplan, D.M., 2015. Linking local retention, self-recruitment, and persistence in marine metapopulations. Ecology 96, 2236–2244. https://doi.org/10.1890/14-1305.1

Lipcius, R.N., Eggleston, D.B., Schreiber, S.J., Seitz, R.D., Shen, J., Sisson, M., Stockhausen, W.T., Wang, H.V., 2008. Importance of Metapopulation Connectivity to Restocking and Restoration of Marine Species. Reviews in Fisheries Science 16, 101–110. https://doi.org/10.1080/10641260701812574

Lowe, W.H., Allendorf, F.W., 2010. What can genetics tell us about population connectivity? Molecular Ecology 19, 3038–3051. https://doi.org/10.1111/j.1365-294X.2010.04688.x

Maritorena, S., d'Andon, O.H.F., Mangin, A., Siegel, D.A., 2010. Merged satellite ocean color data products using a bio-optical model: Characteristics, benefits and issues. Remote Sensing of Environment 114, 1791–1804. https://doi.org/10.1016/j.rse.2010.04.002

Martinez, E., Maamaatuaiahutapu, K., Payri, C., Ganachaud, A., 2007. Turbinaria ornata invasion in the Tuamotu Archipelago, French Polynesia: ocean drift connectivity. Coral Reefs 26, 79–86. https://doi.org/10.1007/s00338-006-0160-3

McPhaden, M.J., Zhang, D., 2004. Pacific Ocean circulation rebounds. Geophysical Research Letters 31. https://doi.org/10.1029/2004GL020727

Mercier, A., Sewell, M.A., Hamel, J.-F., 2013. Pelagic propagule duration and developmental mode: reassessment of a fading link. Global Ecology and Biogeography 22, 517–530. https://doi.org/10.1111/geb.12018

Monaco, C.J., Wethey, D.S., Helmuth, B., 2014. A Dynamic Energy Budget (DEB) Model for the Keystone Predator *Pisaster ochraceus*. PLOS ONE 9, e104658. https://doi.org/10.1371/JOURNAL.PONE.0104658

O'Connor, M.I., Bruno, J.F., Gaines, S.D., Halpern, B.S., Lester, S.E., Kinlan, B.P., Weiss, J.M., 2007. Temperature control of larval dispersal and the implications for marine ecology, evolution, and conservation. Proc. Natl. Acad. Sci. U.S.A. 104, 1266–1271. https://doi.org/10.1073/pnas.0603422104

Onink, V., Wichmann, D., Delandmeter, P., van Sebille, E., 2019. The Role of Ekman Currents, Geostrophy, and Stokes Drift in the Accumulation of Floating Microplastic. Journal of Geophysical Research: Oceans 124, 1474–1490. https://doi.org/10.1029/2018JC014547

Pechenik, J.A., 1990. Delayed metamorphosis by larvae of benthic marine invertebrates: Does it occur? Is there a price to pay? Ophelia 32, 63–94. https://doi.org/10.1080/00785236.1990.10422025

Quinn, B.K., Chassé, J., Rochette, R., 2017. Potential connectivity among American lobster fisheries as a result of larval drift across the species' range in eastern North America. Can. J. Fish. Aquat. Sci. 74, 1549–1563. https://doi.org/10.1139/cjfas-2016-0416

Phillips, J.S., Sen Gupta, A., Senina, I., van Sebille, E., Lange, M., Lehodey, P., Hampton, J., Nicol, S., 2018. An individual-based model of skipjack tuna (Katsuwonus pelamis) movement in the tropical Pacific Ocean. Progress in Oceanography 164, 63–74. https://doi.org/10.1016/j.pocean.2018.04.007

Raapoto, H., Martinez, E., Petrenko, A., Doglioli, A.M., Maes, C., 2018. Modeling the Wake of the Marquesas Archipelago. Journal of Geophysical Research: Oceans 123, 1213–1228. https://doi.org/10.1002/2017JC013285

Raapoto, H., Martinez, E., Petrenko, A., Doglioli, A., Gorgues, T., Sauzède, R., Maamaatuaiahutapu, K., Maes, C., Menkes, C., Lefèvre, J., 2019. Role of Iron in the Marquesas Island Mass Effect. Journal of Geophysical Research: Oceans 124, 7781–7796. https://doi.org/10.1029/2019JC015275

Rahmstorf, S., Coumou, D., 2011. Increase of extreme events in a warming world. Proc. Natl. Acad. Sci. U.S.A. 108, 17905–17909. https://doi.org/10.1073/pnas.1101766108

Raventos, N., Torrado, H., Arthur, R., Alcoverro, T., Macpherson, E., 2021. Temperature reduces fish dispersal as larvae grow faster to their settlement size. Journal of Animal Ecology 90, 1419–1432. https://doi.org/10.1111/1365-2656.13435

Reisser, C., Lo, C., Schikorski, D., Sham Koua, M., Planes, S., Ky, C.L., 2019. Strong genetic isolation of the black-lipped pearl oyster (*Pinctada margaritifera*) in the Marquesas archipelago (French Polynesia). Scientific Reports 2019 9:1 9, 1–12. https://doi.org/10.1038/s41598-019-47729-w

Rodier, M., Longo, S., Henry, K., Ung, A., Lo-Yat, A., Darius, H.T., Viallon, J., Beker, B., Delesalle, B., Chinain, M., 2019. Diversity and toxic potential of algal bloom-forming species from Takaroa lagoon (Tuamotu, French Polynesia): a field and mesocosm study. Aquatic Microbial Ecology 83, 15–34. https://doi.org/10.3354/ame01900

Rougerie, F., Fichez, R., Déjardin, P., 2004. Geomorphology and Hydrogeology of Selected Islands of French Polynesia: Tikehau (Atoll) and Tahiti (Barrier Reef), in: Geology and Hydrogeology of Carbonate Islands. Developments in Sedimentology. Elsevier, pp. 475–502. https://doi.org/10.1016/S0070-4571(04)80037-2

Rougerie, F., Ichez, R., Déjardin, P., 1997. Geomorphology and hydrogeology of selected islands of French Polynesia: Tikehau (atoll) and Tahiti (Barrier reef). Developments in Sedimentology 54.

Sangare, N., Lo-Yat, A., Le Moullac, G., Pecquerie, L., Thomas, Y., Beliaeff, B., Andréfouët, S., 2019. Estimation of physical and physiological performances of blacklip pearl oyster larvae in view of DEB modeling and recruitment assessment. Journal of Experimental Marine Biology and Ecology 512, 42–50. https://doi.org/10.1016/j.jembe.2018.12.008

Sangare, N., Lo-Yat, A., Moullac, G.L., Pecquerie, L., Thomas, Y., Lefebvre, S., Gendre, R.L., Beliaeff, B., Andréfouët, S., 2020. Impact of environmental variability on *Pinctada margaritifera* life-history traits: A full life cycle deb modeling approach. Ecological Modelling 423, 109006. https://doi.org/10.1016/j.ecolmodel.2020.109006

Seebacher, F., White, C.R., Franklin, C.E., 2015. Physiological plasticity increases resilience of ectothermic animals to climate change. Nature Climate Change 5, 61–66. https://doi.org/10.1038/nclimate2457

Selkoe, K.A., Toonen, R.J., 2011. Marine connectivity: a new look at pelagic larval duration and genetic metrics of dispersal. Marine Ecology Progress Series 436, 291–305. https://doi.org/10.3354/meps09238

Shima, J.S., Swearer, S.E., 2009. Larval quality is shaped by matrix effects: implications for connectivity in a marine metapopulation. Ecology 90, 1255–1267. https://doi.org/10.1890/08-0029.1

Sousa, T., Domingos, T., Poggiale, J.-C., Kooijman, S. A. L.M., 2010. Dynamic energy budget theory restores coherence in biology. Philosophical Transactions of the Royal Society B: Biological Sciences 365, 3413–3428. https://doi.org/10.1098/rstb.2010.0166

Tamura, H., Miyazawa, Y., Oey, L.-Y., 2012. The Stokes drift and wave induced-mass flux in the North Pacific. Journal of Geophysical Research: Oceans 117. https://doi.org/10.1029/2012JC008113

Terray, P., 2011. Southern Hemisphere extra-tropical forcing: a new paradigm for El Niño-Southern Oscillation. Clim Dyn 36, 2171–2199. https://doi.org/10.1007/s00382-010-0825-z

Thomas, Y., Dumas, F., Andréfouët, S., 2014. Larval dispersal modeling of pearl oyster pinctada margaritifera following realistic environmental and biological forcing in Ahe atoll lagoon. PLoS ONE 9. https://doi.org/10.1371/journal.pone.0095050

Thomas, Y., Le Gendre, R., Garen, P., Dumas, F., Andréfouët, S., 2012a. Bivalve larvae transport and connectivity within the Ahe atoll lagoon (Tuamotu Archipelago), with application to pearl oyster aquaculture management. Marine Pollution Bulletin 65, 441–452. https://doi.org/10.1016/j.marpolbul.2011.12.027

Thomas, Y., Garen, P., Bennett, A., Le Pennec, M., Clavier, J., 2012b. Multi-scale distribution and dynamics of bivalve larvae in a deep atoll lagoon (Ahe, French Polynesia). Marine Pollution Bulletin, Ahe Atoll and Pearl Oyster Aquaculture in the Tuamotu Archipelago 65, 453–462. https://doi.org/10.1016/j.marpolbul.2011.12.028

Thomas, Y., Garen, P., Pouvreau, S., 2011. Application of a bioenergetic growth model to larvae of the pearl oyster *Pinctada margaritifera* L. Journal of Sea Research, The AquaDEB project (phase II): what we've learned from applying the Dynamic Energy Budget theory on aquatic organisms 66, 331–339. https://doi.org/10.1016/j.seares.2011.04.005

Trakhtenbrot, A., Nathan, R., Perry, G., Richardson, D.M., 2005. The importance of long-distance dispersal in biodiversity conservation. Diversity and Distributions 11, 173–181. https://doi.org/10.1111/j.1366-9516.2005.00156.x

Treml, E.A., Halpin, P.N., Urban, D.L., Pratson, L.F., 2008. Modeling population connectivity by ocean currents, a graph-theoretic approach for marine conservation. Landscape Ecol 23, 19–36. https://doi.org/10.1007/s10980-007-9138-y

Treml, E.A., Roberts, J.J., Chao, Y., Halpin, P.N., Possingham, H.P., Riginos, C., 2012. Reproductive Output and Duration of the Pelagic Larval Stage Determine Seascape-Wide Connectivity of Marine Populations. Integrative and Comparative Biology 52, 525–537. https://doi.org/10.1093/icb/ics101

van Sebille, E., Griffies, S.M., Abernathey, R., Adams, T.P., Berloff, P., Biastoch, A., Blanke, B., Chassignet, E.P., Cheng, Y., Cotter, C.J., Deleersnijder, E., Döös, K., Drake, H.F., Drijfhout, S., Gary, S.F., Heemink, A.W., Kjellsson, J., Koszalka, I.M., Lange, M., Lique, C., MacGilchrist, G.A., Marsh, R., Mayorga Adame, C.G., McAdam, R., Nencioli, F., Paris, C.B., Piggott, M.D., Polton, J.A., Rühs, S., Shah, S.H.A.M., Thomas, M.D., Wang, J., Wolfram, P.J., Zanna, L., Zika, J.D., 2018. Lagrangian ocean analysis: Fundamentals and practices. Ocean Modelling 121, 49–75. https://doi.org/10.1016/j.ocemod.2017.11.008

van Sebille, E., Delandmeter, P., Schofield, J., Hardesty, B.D., Jones, J., Donnelly, A., 2019. Basin-scale sources and pathways of microplastic that ends up in the Galápagos Archipelago. Ocean Science 15, 1341–1349. https://doi.org/10.5194/os-15-1341-2019

Vaughn, C.C., Hoellein, T.J., 2018. Bivalve Impacts in Freshwater and Marine Ecosystems. Annu. Rev. Ecol. Evol. Syst. 49, 183–208. https://doi.org/10.1146/annurev-ecolsys-110617-062703

Wellington, G. M., Victor, B.C., 1989. Planktonic larval duration of one hundred species of Pacific and Atlantic damselfishes (Pomacentridae), Marine Biology.

Williams, P.D., Hastings, A., 2013. Stochastic Dispersal and Population Persistence in Marine Organisms. The American Naturalist 182, 271–282. https://doi.org/10.1086/671059

Wilson, J.R., Harrison, P.L., 1998. Settlement-competency periods of larvae of three species of scleractinian corals. Marine Biology 131, 339–345. https://doi.org/10.1007/s002270050327

Wolanski, E., Richmond, R.H., Golbuu, Y., 2021. Oceanographic chaos and its role in larval self-recruitment and connectivity among fish populations in Micronesia. Estuarine, Coastal and Shelf Science 259, 107461. https://doi.org/10.1016/j.ecss.2021.107461

Wood, S., Baums, I.B., Paris, C.B., Ridgwell, A., Kessler, W.S., Hendy, E.J., 2016. El Niño and coral larval dispersal across the eastern Pacific marine barrier. Nat Commun 7, 12571. https://doi.org/10.1038/ncomms12571

Data Availability. The data that supports the findings of this study and used to train the given model are available from the corresponding author upon reasonable request.

Acknowledgments. The authors acknowledge the Pôle de Calcul et de Données Marines (PCDM; https://wwz.ifremer.fr/en/Research-Technology/Research-Infrastructures/Digital-infrastructures/Computation-Centre) for providing DATARMOR computing and storage resources.

Author contributions. JLL, CJM, SVW and R.L conceived the project and collected the data. HR and RL collected the data and built the physical model. CJM and HR collected the data and run the DEB model. HR, SVW and JLL conducted the analyses of the dispersal data. HR and JLL drafted the manuscript. All authors contributed to the writing and have reviewed the manuscript.

Funding. This work was supported by grant from the Ifremer PinctAdapt project.

Competing interests. The authors declare no competing interests.

Supplementary Materials

985

S1 tab: Indexes of islands assigned following the main current with the name of the cluster to which it belongs and, the average LPP.

Index	Island	Cluster	LPP	Index	Island	Cluster	LPP	Index	Island	Cluster	LPP
1	Hatutu	MAR	12.06	35	Tuanake	TUA3	23.11	69	Maiao	SOC	22.90
2	Eiao	MAR	11.90	36	Motutunga	TUA3	21.85	70	Huahine	SOC	21.04
3	NukuHiva	MAR	12.80	37	Tahanea	TUA3	22.54	71	RaiateaTahaa	SOC	22.33
4	UaHuka	MAR	12.55	38	Faaite	TUA3	21.88	72	BoraBora	SOC	21.36
5	UaPou	MAR	13.15	39	Anaa	TUA3	23.22	73	Tupai	SOC	22.11
6	HivaOa	MAR	13.75	40	Katiu	TUA3	22.71	74	Maupiti	SOC	22.47
7	Mohotane	MAR	12.34	41	Raraka	TUA3	22.40	75	Maupihaa	SOC	24.53
8	Tahuata	MAR	13.11	42	Taiaro	TUA1	21.27	76	PukaPuka	TUA2	19.56
9	FatuHiva	MAR	12.12	43	Kauehi	TUA3	20.22	77	Tatakoto	TUA2	26.49
10	Tepoto	TUA2	19.97	44	Aratika	TUA1	21.11	78	Pukarua	TUA2	23.72
11	Napuka	TUA2	19.88	45	Fakarava	TUA3	20.28	79	Reao	TUA2	23.06
12	Fangatau	TUA2	20.88	46	Toau	TUA1	19.73	80	Akiaki	TUA2	25.80
13	Fakahina	TUA2	22.07	47	Niau	TUA1	20.59	81	Vahitahi	TUA2	26.38
14	Takume	TUA2	21.76	48	Kaukura	TUA1	20.64	82	Nukutavake	TUA2	27.26
15	Raroia	TUA2	22.67	49	Apataki	TUA1	18.06	83	Pinaki	TUA2	27.51
16	Taenga	TUA2	23.31	50	Arutua	TUA1	17.82	84	Vairaatea	TUA2	26.03
17	Nihiru	TUA2	24.13	51	Rangiroa	TUA1	20.51	85	Vanavana	TUA2	29.03
18	Rekareka	TUA2	23.16	52	Tikehau	TUA1	21.55	86	Tureia	TUA2	22.78
19	Tauere	TUA2	23.81	53	Mataiva	TUA1	21.02	87	Moruroa	GAM	27.22
20	Amanu	TUA2	25.69	54	Makatea	TUA1	22.62	88	Fangataufa	GAM	27.46
21	Hao	TUA2	24.22	55	Takaroa	TUA1	20.45	89	Tenararo	GAM	29.12
22	Paraoa	TUA2	25.90	56	Takapoto	TUA1	20.50	90	Vahanga	GAM	29.74
23	Ahunui	TUA2	26.27	57	Tikei	TUA1	21.34	91	Tenarunga	GAM	30.12
24	Manuhangi	TUA2	26.41	58	Manihi	TUA1	21.51	92	Matureivavao	GAM	29.27
25	NengoNengo	TUA2	25.86	59	Ahe	TUA1	20.26	93	MaruteaSud	GAM	28.44
26	RavahereMarokau	TUA2	25.28	60	Anuanuraro	GAM	27.56	94	Maria	GAM	30.94
27	Reitoru	TUA2	25.19	61	Anuanurunga	GAM	28.65	95	Mangareva	GAM	21.77
28	Hikueru	TUA2	23.23	62	Nukutepipi	GAM	27.95	96	Temoe	GAM	26.20
29	Tekokota	TUA2	24.02	63	Hereheretue	GAM	24.59	97	Morane	GAM	30.93
30	Haraiki	TUA3	23.74	64	Tematangi	GAM	27.72	98	Rimatara	AUS1	30.78
31	MaruteaNord	TUA2	23.95	65	Mehetia	SOC	23.38	99	Rurutu	AUS1	29.31
32	Makemo	TUA2	23.38	66	Tetiaroa	SOC	22.00	100	Tubuai	AUS1	27.14
33	TepotoSud	TUA3	22.26	67	Tahiti	SOC	23.15	101	Raivavae	AUS1	30.41
34	Hiti	TUA3	23.83	68	Moorea	SOC	22.70	102	Rapa	AUS2	28.22

*FILE ANIMATION

S2 File. Animation of the modelled dispersal paths for a duration of 35 days without settlement on FP, expressed as larval densities and calculated as the number of particles in each cell on a 1/100° grid.

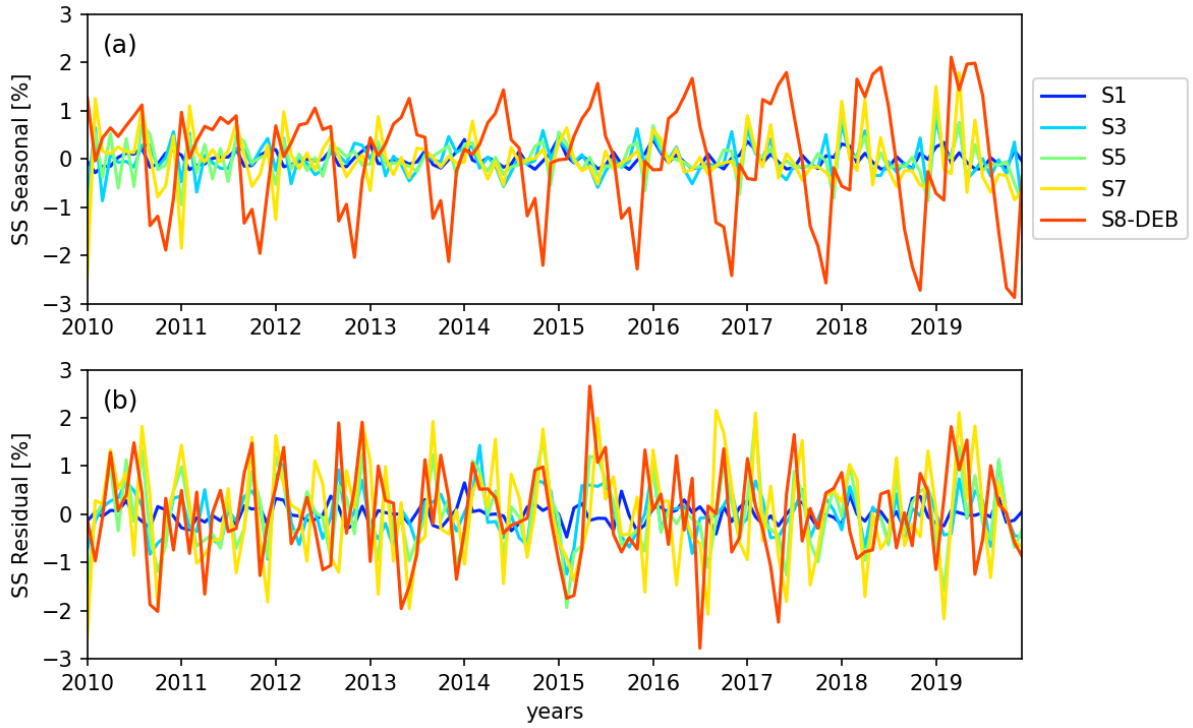

S3 Fig. (a) Seasonal and (b) residual settlement success (SS) extracted from the STL over the full dataset (all archipelagos included). For ease of representation, only scenarios 1, 3, 5, 7 and 8 are represented in blue, light blue, green, yellow and orange, respectively.